EYE-CLIMA
Verifying emissions of climate forcers

Preliminary fluxes of CO_2, CH_4 and N_2O at 0.2° from 2018

DELIVERABLE D3.3

Author(s):	CEA: Grégoire Broquet, Antoine Berchet Science Partners: Audrey Fortems-Cheiney FMI: Anteneh Getachew Mengistu, Tuula Aalto, NILU: Nalini Krishnankutty

Date of submission:	19-09-2024
Version:	1.0
Responsible partner:	CEA
Deliverable due date:	30-06-2024
Dissemination level:	Public

Call:	HORIZON-CL5-2022-D1-02
Topic:	Climate Sciences and Responses
Project Type:	Research and Innovation Action
Lead Beneficiary:	NILU - Norsk Institutt for Luftforskning

This project has received funding from the European Union's Horizon Europe research and innovation programme under grant agreement No 101081395

Document History

Version	Date	Comment	Modifications made by
0.1	16-09-2024	First draft	Grégoire Broquet, Antoine Berchet, Audrey Fortems-Cheiney, Anteneh Getachew Mengistu, Tuula Aalto, and Nalini Krishnankutty
0.2	17-09-2024	Internal review	Rona Thompson
0.3	19-09-2024	Final version	Grégoire Broquet, Antoine Berchet, Audrey Fortems-Cheiney, Anteneh Getachew Mengistu, Tuula Aalto, and Nalini Krishnankutty
1.0	19-09-2024	Submitted to Commission	Rona Thompson

This project has received funding from the European Union's Horizon Europe research and innovation programme under grant agreement No 101081395

Summary

One of the main objectives of EYE-CLIMA is to support the verification of National Greenhouse Gas Inventories (NGHGIs) by providing estimates of greenhouse gas emissions based on atmospheric observations. Emissions estimates can be derived from observations through atmospheric inversions, and the use of this method to verify NGHGIs has been highlighted in the 2019 refinement of the IPCC Guidelines. However, the adoption of this type of verification has been hampered by the complexity of the method, the uncertainties and, hitherto, the limited resolution of the emission estimates.

EYE-CLIMA has a strong focus on improving both the accuracy and resolution of regional inversions. The accuracy of emissions derived from atmospheric inversions is expected to improve with higher spatial resolution due to improved resolution of the atmospheric transport, which should enable a better representation of the observations, as well as improved resolution of the fluxes (together reducing the model representation error). Moreover, higher spatial resolution will enable the borders of countries to be more accurately resolved. However, the higher spatial resolution presents several challenges.

In this context, the main objective of this preliminary deliverable is to assess the performance and computational cost of inversions run at higher spatial resolution, specifically 0.2°×0.2°. A follow-up deliverable (due in 2025) will extend the inversions to cover at least the period 2018 to 2023. The inversions at this resolution will not be extended further back in time than the start of the ICOS atmospheric record (or for CH_4 the launch of the TROPOMI instrument onboard the satellite Sentinel 5P) because prior to the start of these records the observation coverage over Europe is poorer.

This deliverable presents the first results of the high-resolution (0.2°) regional inversions for CO_2, CH_4 and N_2O fluxes in Europe. CH_4 inversions cover the period from 2017 to 2022 and N_2O inversion results are shown for 2018. For CO_2, an assessment of the impact of the higher resolution transport model on the simulated CO_2 mole fractions, and the associated computational cost, is presented for the month of June 2019.

For CH_4, the total emissions are optimised in this preliminary deliverable. The inversion results in large increases in Central Europe, large reductions in Italy, Romania and UK, and modest reductions in northern Europe during summer, compared to the prior flux estimates. The emission reductions in southern Europe are most probably due to a too large prior estimate for geological emissions.

For N_2O, the optimised emissions show an overall reduction in the emissions (~21%) compared to the prior estimate. Most of the reductions in emissions are concentrated near Italy, in Central and Eastern Europe, while there are some regions, particularly in Northwestern Europe (such as the UK and parts of France) and regions around Netherlands where the emissions increased.

For CO_2, first comparisons over the month of June 2019 do not show a clear improvement, even a slight deterioration, of the fit to surface measurements with the simulation at relatively high resolution compared to the one at 0.5°. However, a full and detailed assessment of the potential of having a 0.2° resolution would have benefited from longer experiment, but this is currently hampered by a high computational cost. The very high computational cost indeed makes it difficult to perform experiments over longer periods at this stage. Technical developments on CHIMERE, particularly by porting the code to GPU-compatible environment, are currently in progress.

This project has received funding from the European Union's Horizon Europe research and innovation programme under grant agreement No 101081395

TABLE OF CONTENTS

This project has received funding from the European Union's Horizon Europe research and innovation programme under grant agreement No 101081395

1. Introduction

One of the main objectives in EYE-CLIMA is to address the need for independent verification of National Greenhouse Gas Inventories (NGHGIs) by developing top-down methods based on atmospheric inversion (using both satellite remote sensing and ground-based observations) to a level of readiness where they can be used to determine emissions at national and sub-national scales. Towards this objective, this deliverable presents first results of atmospheric inversions of CO_2, CH_4 and N_2O run at a spatial resolution of 0.2°×0.2° over Europe, focusing on EU27 countries plus UK, Switzerland and Norway (EU27+3).

Atmospheric inversions are a valuable method to constrain emission estimates using observations of atmospheric mole fractions. The method involves using an atmospheric chemistry transport model (ACTM) to relate an existing independent estimate of the fluxes (the prior estimate) to atmospheric mixing ratios and to determine the model-observation error. This error is then used to update the prior estimate by effectively inverting the transport to relate the difference in mixing ratio to a difference in flux.

Although the atmospheric inversion methodology is well-established there is still room for substantial improvements. The spatial resolution of regional inversions prior to EYE-CLIMA was typically around 0.5° (e.g. EUROCOM, VERIFY and RECCAP-2), but improving the resolution should improve the representation of observations by the atmospheric transport model, and it will improve the resolution of the fluxes, together resulting in a reduction of the model representation error.

The overall aim of this deliverable, and its follow-up (D3.4 due in 2025), is to perform European inversions for CO_2, CH_4 and N_2O for at least the period 2018 to 2023, i.e., when there are sufficiently dense observations (when observations are available from ICOS, OCO-2 for CO_2 and from TROPOMI for CH_4).

The inversions are performed using the Community Inversion Framework (CIF) combined with the FLEXPART or CHIMERE models.

2. Methodology

2.1. Inversion framework

The Community Inversion Framework (CIF) is an open-source inversion framework and was developed with the intention of concentrating inversion developments into a community code and to be interfaced with different atmospheric transport models (Berchet et al., 2021). In EYE-CLIMA, the CIF is interfaced with two atmospheric transport models, FLEXPART and CHIMERE (see Section 2.2).

For the high-resolution inversions, we use the Community Inversion Framework's (CIF) four-dimensional variational (4DVAR) optimization approach (Berchet et al., 2021). The inversion algorithm minimizes the following cost function $J(\mathbf{x})$ with respect to the state vector $\mathbf{x}$:

$$J(\boldsymbol{x}) = \frac{1}{2}(\boldsymbol{x} - \boldsymbol{x_b})^{\mathrm{T}}\mathbf{B}^{-1}(\boldsymbol{x} - \boldsymbol{x_b}) + \frac{1}{2}(H(\boldsymbol{x}) - \boldsymbol{y})^{\mathrm{T}}\mathbf{R}^{-1}(H(\boldsymbol{x}) - \boldsymbol{y}) \quad (1)$$

Here, $\mathbf{x}$ represents the state vector of model variables, $\mathbf{x_b}$ is the initial guess or prior state vector, $\mathbf{B}$ denotes the background error covariance matrix reflecting uncertainties in $\mathbf{x_b}$, $\mathbf{y}$ is the vector of observed data, $H(\mathbf{x})$ is the observation operator mapping $\mathbf{x}$ to the observation space, and $\mathbf{R}$ is the observation

This project has received funding from the European Union's Horizon Europe research and innovation programme under grant agreement No 101081395

error covariance matrix accounting for uncertainties in **y**. The first term on the right-hand side of Eq. 1 accounts for deviation from the prior state $\mathbf{x_b}$ and second term represents the observational constraints on the prior fluxes.

To minimize $J(\mathbf{x})$, the gradient $\nabla J(\mathbf{x})$ is computed:

$$\nabla J(\boldsymbol{x}) = \mathbf{B}^{-1}(\boldsymbol{x} - \boldsymbol{x_b}) + H'(\boldsymbol{x})\mathbf{R}^{-1}(H(\boldsymbol{x}) - \boldsymbol{y}) \quad (2)$$

The conjugate gradient algorithm (Lanczos, 1950) utilizes $\nabla J(\mathbf{x})$ to iteratively update **x**, continuing until the gradient norm falls below a predefined threshold or a maximum number of iterations is reached.

2.2. Atmospheric transport models

In this deliverable, two different atmospheric transport models are used, the Lagrangian Particle Dispersion Model (LPMD), FLEXPART, and the regional Eulerian model, CHIMERE. These models are described below.

2.2.1. FLEXPART

FLEXPART models the dispersion and turbulent mixing of gases and aerosols in the atmosphere using virtual particles (Stohl et al. in 1995; Pisso et al. in 2019). In this deliverable, two versions of FLEXPART are used, i.e., v10.4 and v11 (released 2024). One of the main differences in v11 is the possibility to perform the transport calculations on the original grid of the meteorological input fields, which brings some improvements to the accuracy. In this study, the meteorological reanalysis data from the European Centre for Medium-Range Weather Forecasts (ECMWF) ERA5 (Hittmeir et al. 2018) is used to drive FLEXPART. The ERA5 data are available at hourly intervals and span 137 vertical layers.

FLEXPART is run to generate source-receptor relationships (SRRs), which describe the relationship between change in observed mixing ratio and the fluxes. The SRRs are used in the inversion framework (CIF) to model atmospheric mixing ratios as well as to relate the model-observation differences to a correction to the prior fluxes.

For each observation, a 10-day backward transport simulation is made using the FLEXPART to produce the SRRs. These SRRs are saved with a resolution of 0.2°×0.2° for the nested domain over Europe, and at 2°×2° for the global domain, all of which are stored at hourly intervals. For atmospheric greenhouse gases like CH_4 and N_2O which have long atmospheric lifetime, a background mixing ratio estimate is needed, which accounts for the influence on the observation prior to the start of the backward trajectory calculation. This is determined by coupling the end points of the particle trajectories to 3D initial mixing ratio fields of the target species, which may be obtained from a global model (Thompson and Stohl, 2014).

2.2.2. CHIMERE

CHIMERE is an Eulerian chemistry-transport model (Menut et al., 2013; Mailler et al., 2017). The specific configuration, used here for the simulations of CO_2 concentrations and for the quantification of the terrestrial ecosystem at the relatively high spatial resolution of 0.2° over Europe, is detailed in Section 5.

This project has received funding from the European Union's Horizon Europe research and innovation programme under grant agreement No 101081395

3. CH_4 inversions

This section describes the CIF-FLEXPART CH_4 inversion configuration for Europe. For calculating the background mixing ratios, the FLEXPART trajectories are coupled to 3D CH_4 mixing ratios fields from the CAMS (v22r2) global CH_4 inversion (https://ads.atmosphere.copernicus.eu/cdsapp#!/dataset/cams-global-greenhouse-gas-inversion?tab=overview). We have defined the region boundary of the CH_4 nested domain to align with JSBACH-HIMMELI, which is used for the prior estimate of the CH_4 land biosphere flux. The region is specified as: longitude ranging from 12°W to 37°E and latitude ranging from 35°N to 73°N. For each CH_4 observation, a 10-day backward transport simulation is made using the FLEXPART to produce the SRRs.

3.1. Prior fluxes

To generate comprehensive prior CH_4 emission estimates, we incorporate monthly data from major source categories: anthropogenic, biomass burning, land-biosphere (natural), as well as climatological estimates for ocean, geological, and termite emissions. These datasets are aggregated to provide a net total prior flux estimate. Our monthly prior flux data for anthropogenic emissions is from GAINS for EU27+3 countries (D2.8) and EDGAR v8.0 elsewhere (hereafter, GAINS-EDGAR). Monthly prior emission estimates for fire emissions are obtained from GFEDv4.1 (Randerson et al., 2017), excluding agricultural waste burning as it is encompassed in our anthropogenic emissions. Land biosphere emission estimates within our study domain (Europe) are derived from the JSBACH-HIMMELI ecosystem model (D2.3). These emissions are the aggregated emissions from peat, inundated soil, and net mineral soil as calculated by JSBACH-HIMMELI (hereafter JSBACH), The JSBACH–HIMMELI model framework, which combines JSBACH with the HIMMELI model for northern peatland emissions, provides wetland and mineral soil CH_4 fluxes daily and at a spatial resolution of 0.1°×0.1°. For the ocean prior flux, we utilize climatological estimates of ocean emissions from the work of Weber et al. (2019). Geological prior emissions are derived from Etiope et al. (2019) globally scaled to 23 Tg/y (Saunois et al., 2024). Lastly, prior termite emissions are based on Saunois et al. (2024).

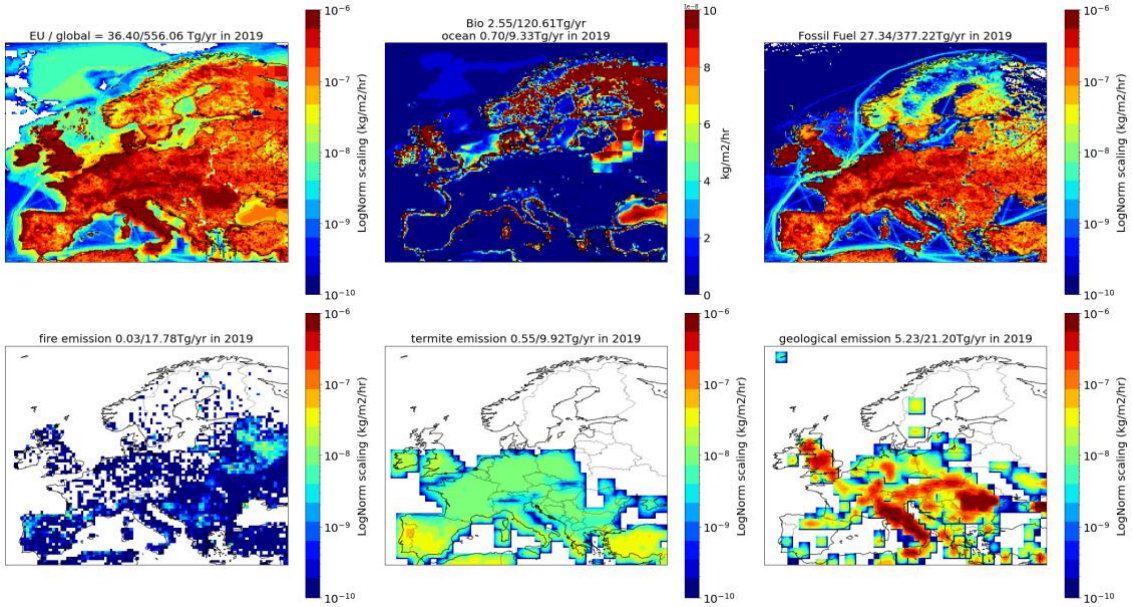

Figure 3.1: Annual mean methane emissions by source and for the total. The title of each subplot indicates the source and provides annual emission estimates for the domain and globally in Tg/yr. Note that the colour-scales of the maps vary.

This project has received funding from the European Union's Horizon Europe research and innovation programme under grant agreement No 101081395

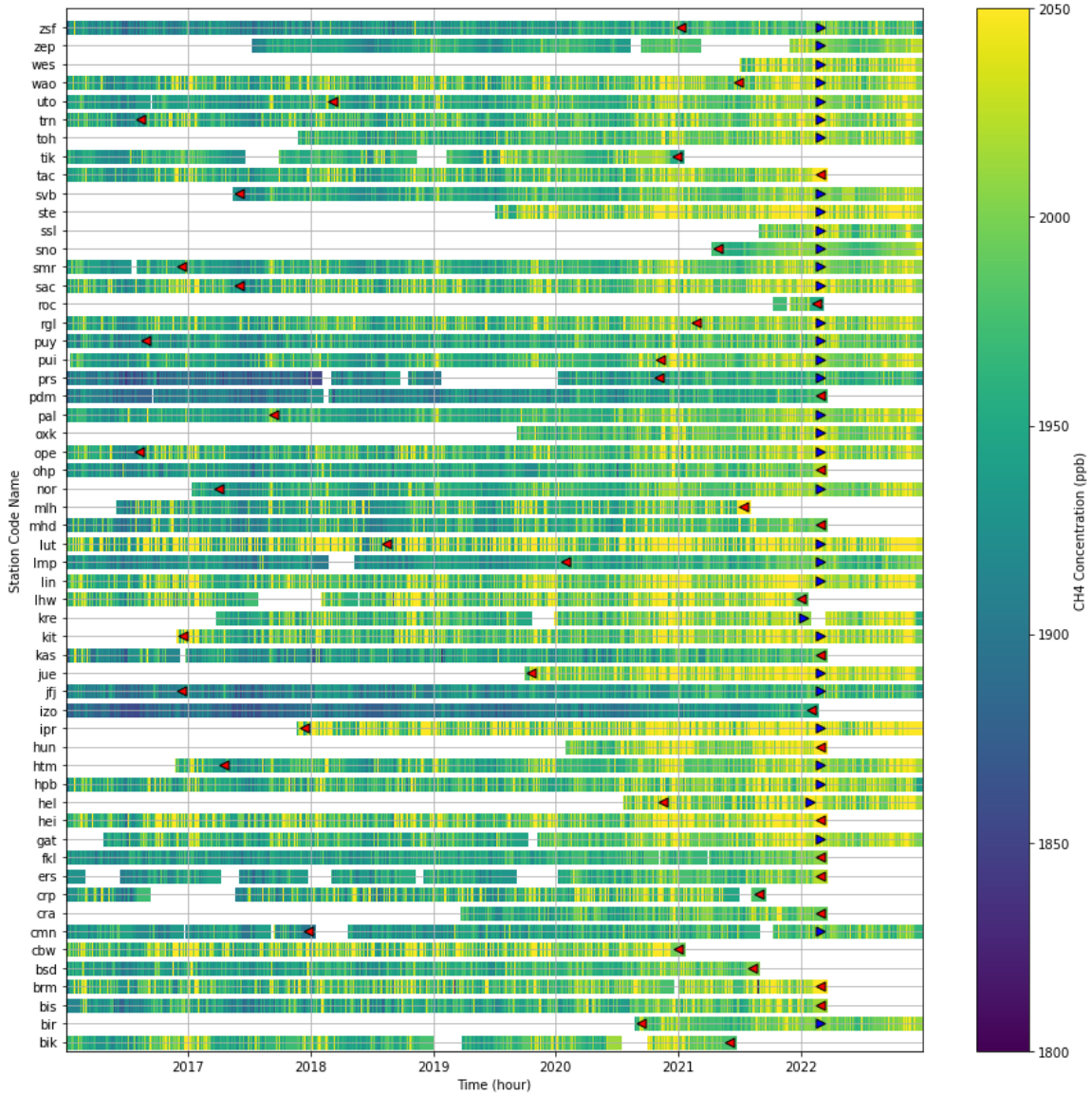

Figure 3.2: Overview of observational data density from 2016 to 2022 and ICOS levelling. Data before the red triangle represents non-ICOS data processed only by site PIs. Data between the red and blue triangles represents the final ICOS QC (Quality Control) data. Data after the blue triangle indicates ICOS real-time data. White gaps indicate periods with no data available. The colour bar indicates observed CH_4 concentration in ppb, with each station represented by a 3-letter code on the y-axis.

3.2. Observations

The Integrated Carbon Observation System (ICOS) offers a European compilation of atmospheric CH_4 mole fraction time series data. These datasets include both quality-controlled ICOS-labelled and non-labelled datasets. For data density and ICOS labelling see Figure 3.2. To strengthen observational constraint, we incorporated data from 45+ in-situ measurements sourced from the Obspack GLOBALVIEWplusv8.0 Europe CH_4 time series (Schuldt et al., 1983–2021) (https://meta.icos-cp.eu/objects/ wIrU4_bb2C74AI01I3d9WyzB, last accessed on March 17, 2024). Their geographical distribution across Europe is depicted in Figure 3.3. In cases where multiple intake heights were available, such as at the Cabauw station with intake heights at 27, 67, 127, and 207 meters above ground level, we opted to assimilate data solely from the highest intake height. This approach was taken to ensure that the assimilated data represent well-mixed conditions and not just very local influences. We

This project has received funding from the European Union's Horizon Europe research and innovation programme under grant agreement No 101081395

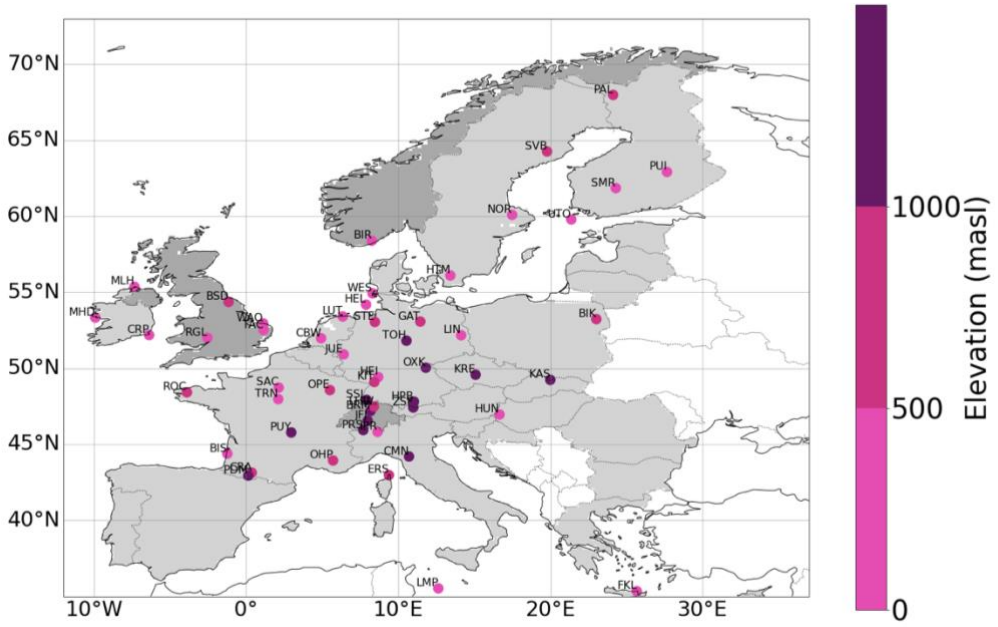

Figure 3.3: Geographic distribution of sites used in data assimilation. Grey areas represent the EU27 countries, while dark grey indicates the +3 countries. The colour bar shows site elevations in meters above sea level (m.a.s.l.).

assimilate hourly observations between 14:00 - 16:00 for low altitude stations (<= 1000 m.a.s.l) and between 00:02 - 04:00 for high-altitude stations (> 1000 m.a.s.l).

3.3 Results

3.3.1 Comparison of Modelled and observed CH_4 mixing ratio

The inversion covers the period from 2017 to 2022. Figure 3.4. displays a sample time series of CH_4 measurements from four stations: Cabauw in the Netherlands, Lindenberg in Germany, Pallas in Finland and Steinkimmen in Germany accompanied by both the prior and posterior estimates generated through the CIF-FLEXPART inversion. The results clearly illustrate that the posterior estimates exhibit a significantly improved alignment with the observed time series, emphasizing the effectiveness of the data assimilation process. In Figure 3.5., we provide root mean square error (RMSE), bias, and correlation metrics for both the prior and posterior estimates for all the observation sites used in our inversion system. A posteriori, they exhibit lower bias and RMSE values while demonstrating a notably higher level of correlation with the observed data.

This project has received funding from the European Union's Horizon Europe research and innovation programme under grant agreement No 101081395

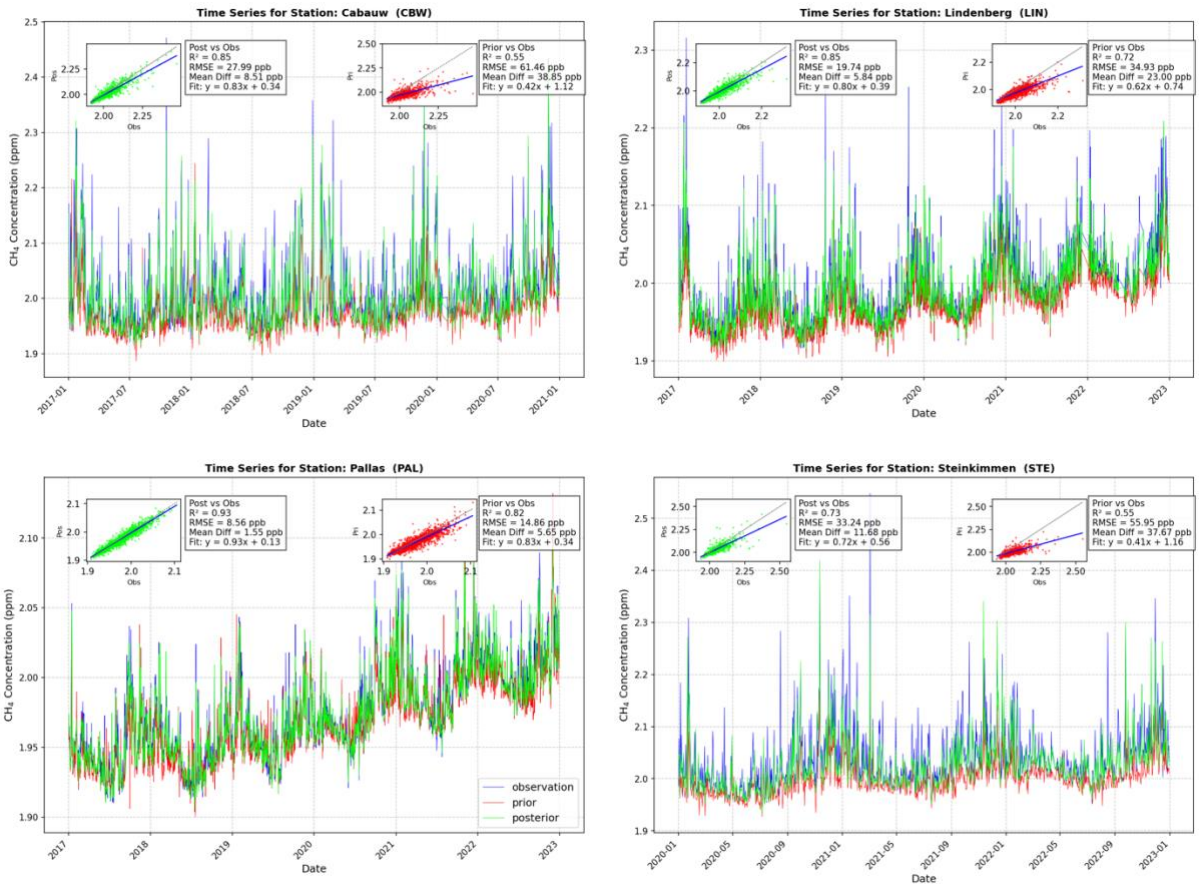

Figure 3.4: Time series of assimilated CH_4 concentration sampled four stations Cabauw in The Netherlands Lindenberg in Germany, Pallas in Finland and Steinkimmen in Germany: assimilated Obspack Measurement (blue), CIF-FLEXPART Inversion results for posterior concentration (green), and prior concentration (red)

This project has received funding from the European Union's Horizon Europe research and innovation programme under grant agreement No 101081395

Figure 3.5: Overview of statistical results for assimilated observed concentration and CIF-FLEXPART posterior and prior simulated concentrations from all stations used in the inversion: a) six years mean bias (observation – simulated concentration); b) RMSE; and c) Correlation.

3.3.2 Spatial distribution of prior and posterior fluxes

The posterior estimated total CH_4 emissions for the EU27+3 is 23.18 Tg/yr. This represents a slight increase compared to the prior estimate, which was 21.75 Tg/yr. Figure 3.6 presents seasonal mean posterior and prior estimates, along with their differences, illustrating significant variations across geographical regions.

This project has received funding from the European Union's Horizon Europe research and innovation programme under grant agreement No 101081395

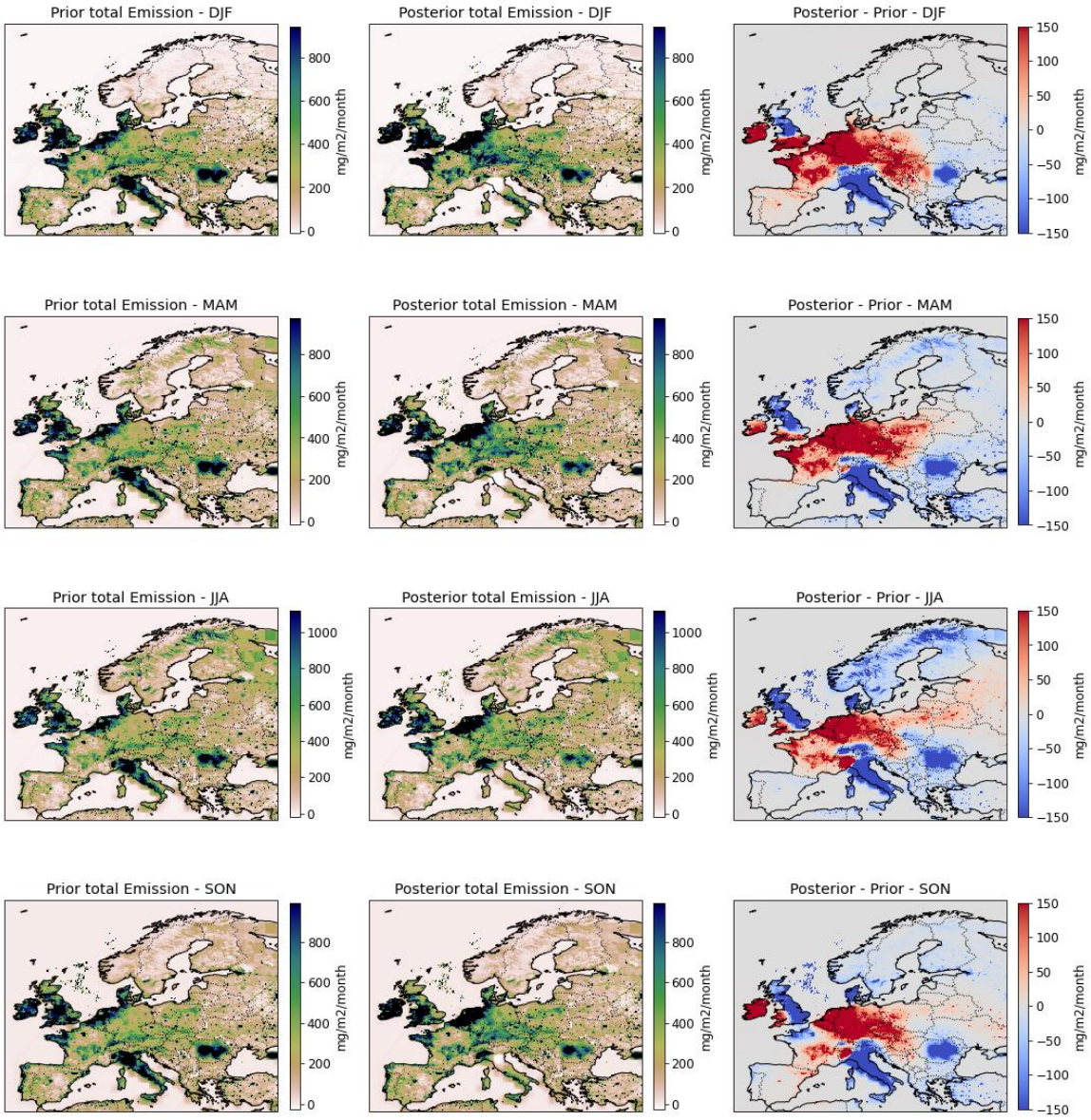

Figure 3.6: Seasonal mean spatial distribution of CH_4 estimates from CIF-FLEXPART inversion at a higher resolution of 0.2°× 0.2° grid in the year 2019: prior (left panel), posterior (middle panel) and posterior increments computed as (posterior – prior) (right panel).

In central Europe, the posterior CH_4 flux shows a notable increase compared to prior estimates, while in Italy, Romania, and the UK a reduction is seen. This reduction is likely due to overestimated prior values influenced by too high geological emission estimates (see Figure 3.1). Similar spatial patterns in posterior CH_4 flux estimates have also been observed in previous studies (e.g. Bergamaschi et al., 2018; Saunois et al., 2024, Petrescu et al., 2021). In Scandinavian countries, the figure indicates a marked reduction in summer (June-August) in the fluxes compared to the prior, which can be attributed to the prior overestimating the summer fluxes in these northernmost regions of Europe. However, wetland methane fluxes show also some increases in the region.

This project has received funding from the European Union's Horizon Europe research and innovation programme under grant agreement No 101081395

4. N_2O inversions

This section describes the CIF-FLEXPART inversion configuration for N_2O over Europe. For N_2O the nested domain boundary is defined: longitude ranging from 11°W to 35°E and latitude ranging from 34°N to 72°N.

4.1 Model set-up

For the N_2O inversions, FLEXPART-v11 was modified to produce output for two nested domains (at 0.5° and 0.2°) from the same run, improving the computational cost of running the model for inversions at two different resolutions.

A variable-resolution grid was defined for the inversion as shown in Figure 4.1. The grid is defined based on the SRRs and the prior fluxes following the method of Thompson and Stohl (2014). The grid cells in the domain correspond to aggregates of 1.6°, 0.8°, 0.4°, and 0.2° resolution. Here, grid cells are aggregated where there is little information provided by the observations about the fluxes. Using an aggregated grid has the advantage of reducing the dimension of the inversion problem, thus reducing the computation time and memory required, while avoiding introducing aggregation error.

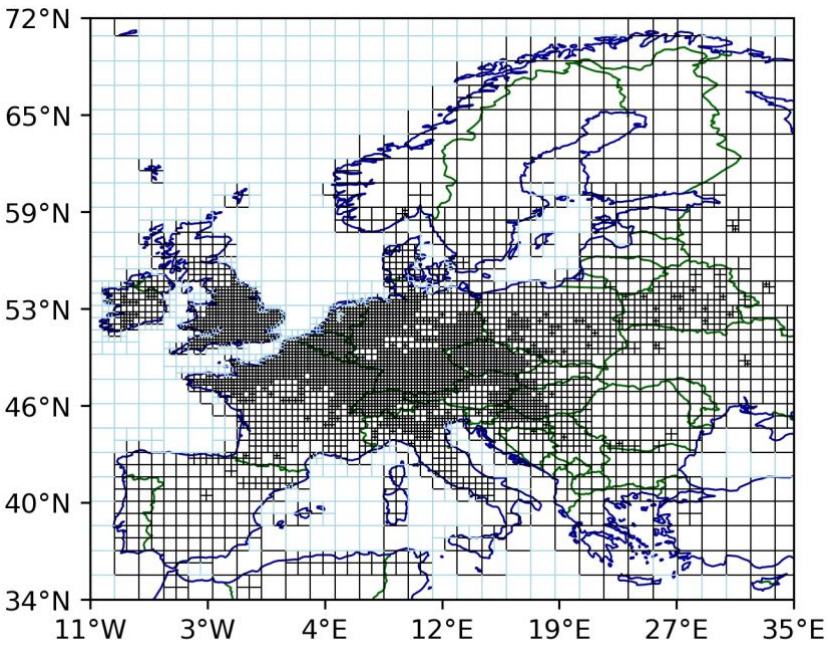

Figure 4.1: Variable-resolution grid used in the inversion

4.2. Prior Fluxes

In the prior flux estimate, we incorporate monthly data for the following sources: agriculture, other anthropogenic emissions, biomass burning, emissions from "natural" soils, as well as climatological estimates for ocean emissions. Our monthly prior flux data for agriculture and other anthropogenic emissions is from GAINS (D2.8) for EU27+3 countries. Agricultural emissions include direct and indirect emissions, as well as manure. Other anthropogenic emissions from GAINS include those of transport, industrial and waste. Monthly prior emission estimates for the biomass burning emissions are obtained from GFEDv4.1 (Randerson et al., 2017), excluding agricultural waste burning as it is encompassed in our agricultural emissions. Natural emissions (i.e., from unmanaged soils) were taken from the O-CN

This project has received funding from the European Union's Horizon Europe research and innovation programme under grant agreement No 101081395

land surface model. We utilize climatological estimates of ocean emissions from PlankTOM model for ocean prior flux. Prior N_2O emissions from different sources used in the inversion are shown in Figure 4.2. However, the inversion optimises the total emissions combined from all the sources.

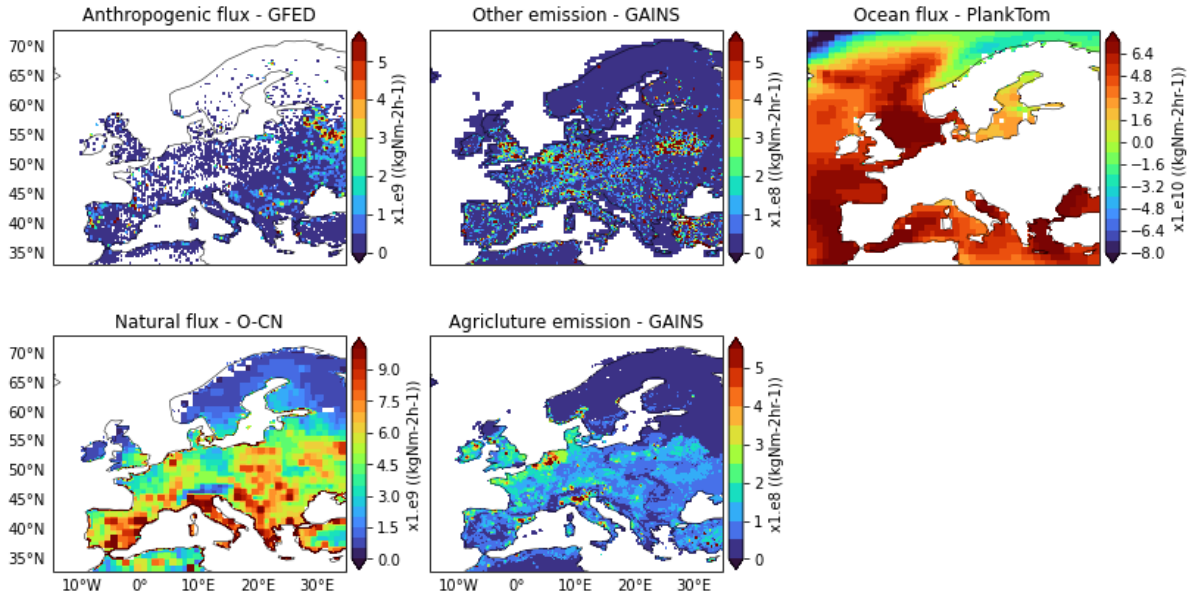

Figure 4.2: Annual mean N_2O emissions at 0.1°x0.1° resolution for 2019. Note that the scales of the maps vary

4.3 Observations

The N_2O observations for Europe were compiled through a collaboration of EYE-CLIMA with the AVENGERS and PARIS projects. We incorporated data from 30 sites that have valid observations from 2018. The data are from the InGOS project (pre-ICOS), the ICOS network, the World Data Centre for Greenhouse Gases (WDCGG), and the NOAA discrete (flask) sampling network (Henne et al., 2024), https://meta.icos-cp.eu/collections/FHIS-w3c_eny9-NDoR7ddvTX. The geographical distribution of sites across Europe is depicted in Figure 4.3. In cases where multiple intake heights were available, we opted to assimilate data solely from the highest intake height. This approach ensured that the assimilated data represented the uppermost atmospheric layer. We assimilate hourly observations for all the sites.

The altitude of observation sites vary from sea level to as high as ~2500 masl. However, the orography in the meteorological data used in the transport model is only resolved at 0.5° and thus the altitude of the mountain sites in the model will be lower than in reality. Hence, the particle release heights in FLEXPART have been adjusted for the mountain sites (defined as > 1000 masl), to be the mid-point between the actual altitude of the sites and the altitude given by the meteorology. Figure 4.4. shows for each site how many months of data are available for a given year for the whole inversion period (2018-2023).

This project has received funding from the European Union's Horizon Europe research and innovation programme under grant agreement No 101081395

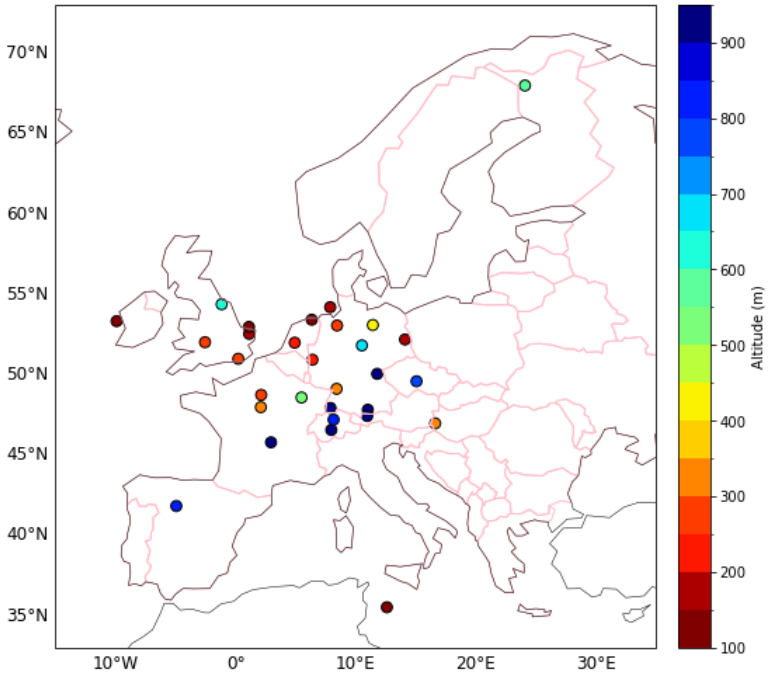

Figure 4.3: Geographical distribution of the sites showing also their altitude

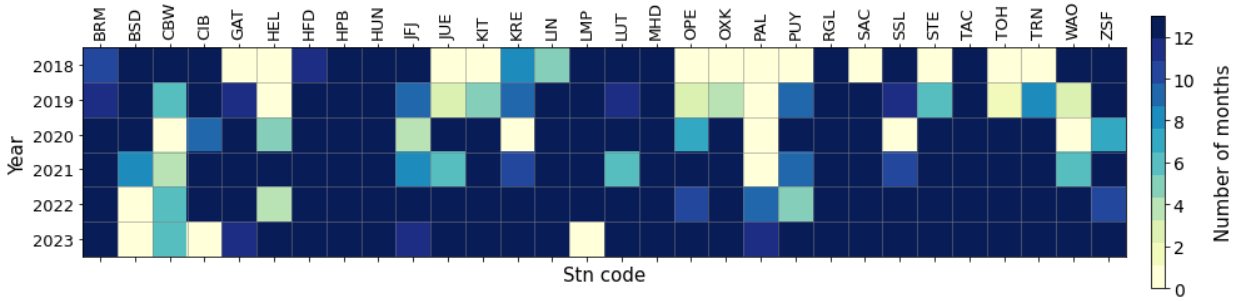

Figure 4.4: Data density in months for each site per year

4.4 Results

Here, we discuss the high-resolution inversion results for the year 2018.

4.4.1 Comparison of modelled and observed atmospheric N_2O mole fractions

Figure 4.5 shows the daily time series of N_2O mole fractions at four stations used in the inversion with the prior and posterior estimates obtained from CIF-FLEXPART. The results illustrate that after inversion the mole fractions show improved agreement with the observed time series compared to the prior. Figure 4.6 shows the statistical analysis of mole fractions estimated from CIF-FLEXPART with observations. The correlation of prior and posterior mixing ratios with observations are shown for each site used in the inversion. At most of the sites, the correlations are better than 60% for both prior and posterior mole fractions. Also, it is evident that the posterior estimates are better correlated with observations than the prior for most of the sites. The RMSE for posterior simulations are smaller than or equal to the RMSE for prior simulations. This indicates that posterior simulations generally show an improvement in prediction accuracy over prior simulations.

This project has received funding from the European Union's Horizon Europe research and innovation programme under grant agreement No 101081395

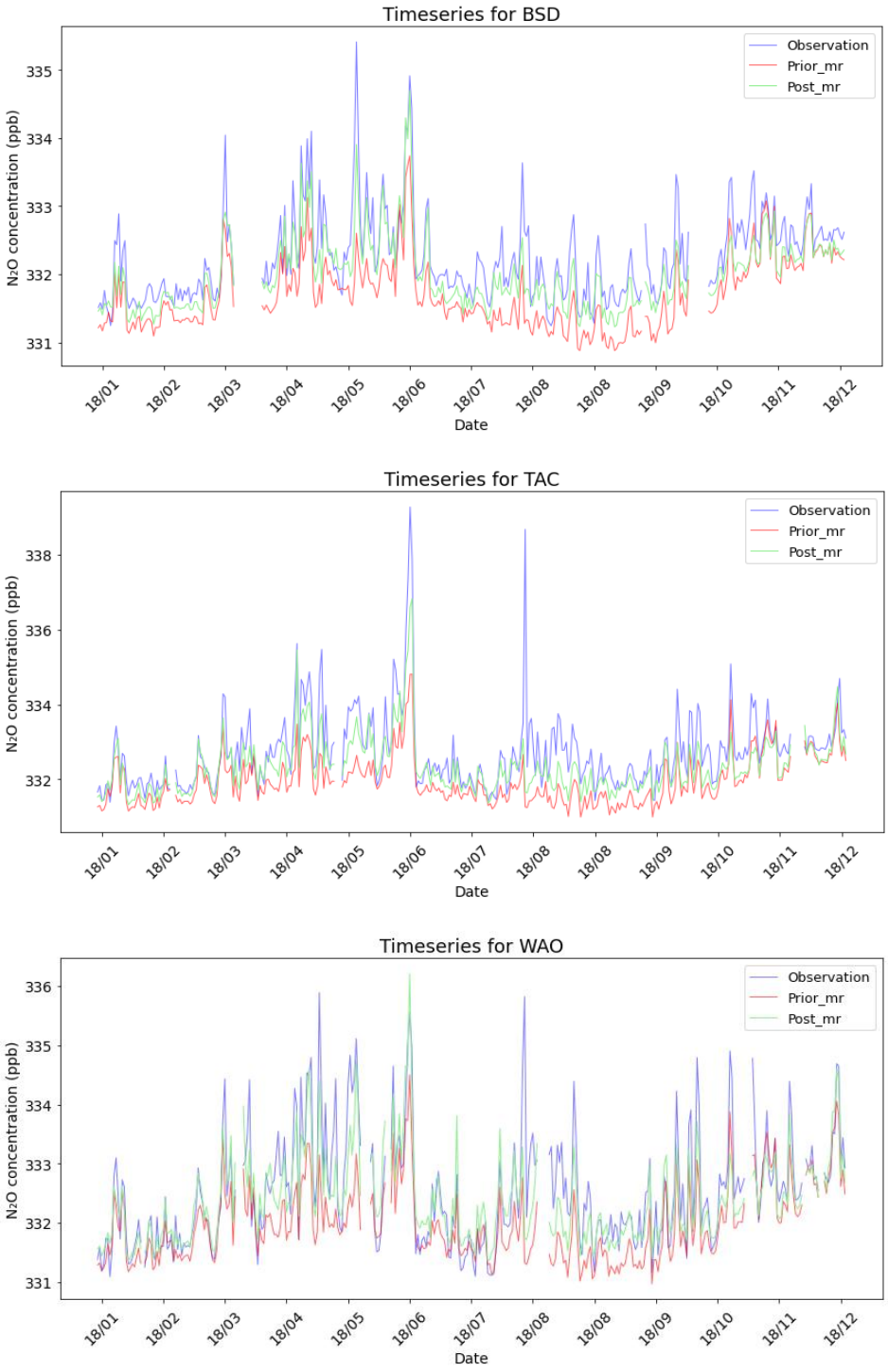

Figure 4.5: Time series of assimilated N_2O concentrations sampled at different stations used in the inversion for the year 2018. Assimilated measurement (blue), CIF-FLEXPART Inversion results for posterior concentration (green), and prior concentration (red).

This project has received funding from the European Union's Horizon Europe research and innovation programme under grant agreement No 101081395

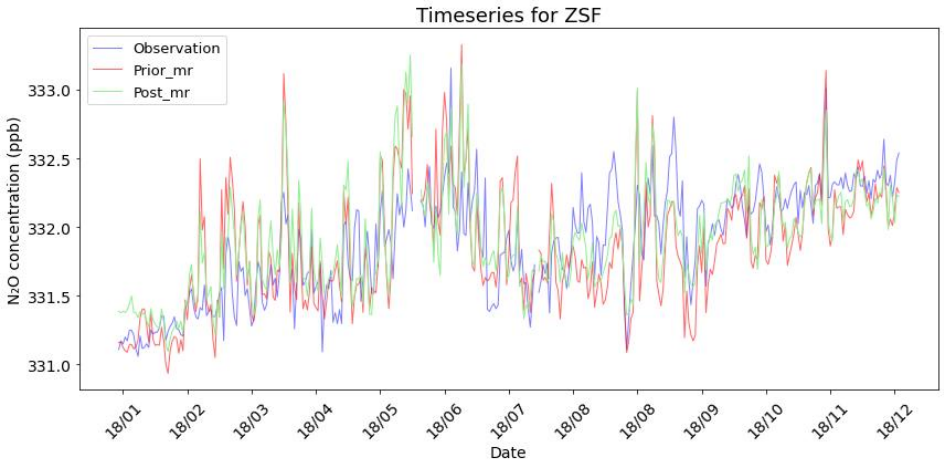

Figure 4.5: continued.

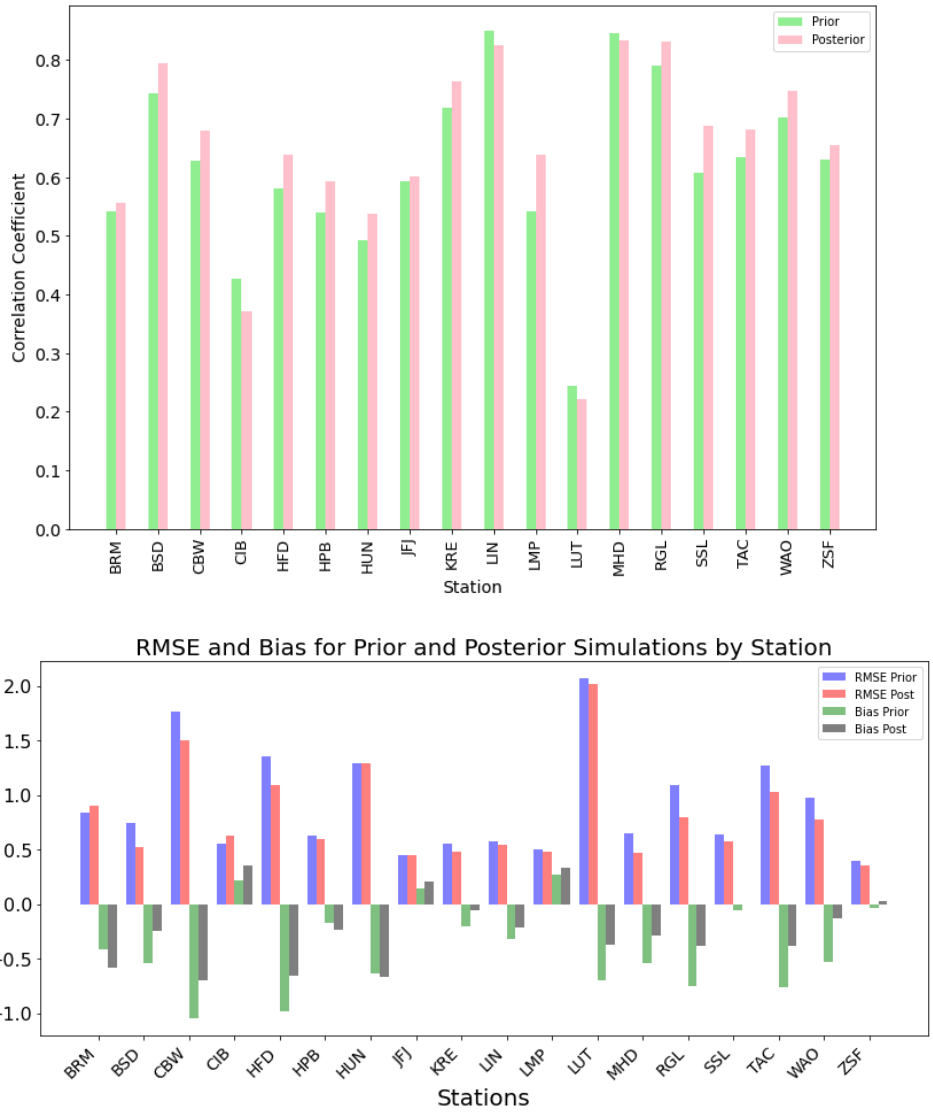

Figure 4.6: Statistical analysis of prior and posterior concentrations with observations

This project has received funding from the European Union's Horizon Europe research and innovation programme under grant agreement No 101081395

4.4.2. Spatial distribution of prior and posterior fluxes

Figure 4.7 shows the spatial distribution of N_2O emissions and their differences over Europe for 2018. The comparison between the prior and posterior emissions indicates a decrease in the total estimated N_2O emissions after inversion (from 1.310 Tg/yr to 1.041 Tg/yr). This amounts to ~21% decrease in the total emissions. The bottom figure shows the difference between the posterior and prior N_2O emissions across Europe. Most of the reductions in emissions are concentrated near Italy, in Central and Eastern Europe, while there are some regions, particularly in Northwestern Europe (such as the UK and parts of France) and regions around the Netherlands where the emissions estimates increased.

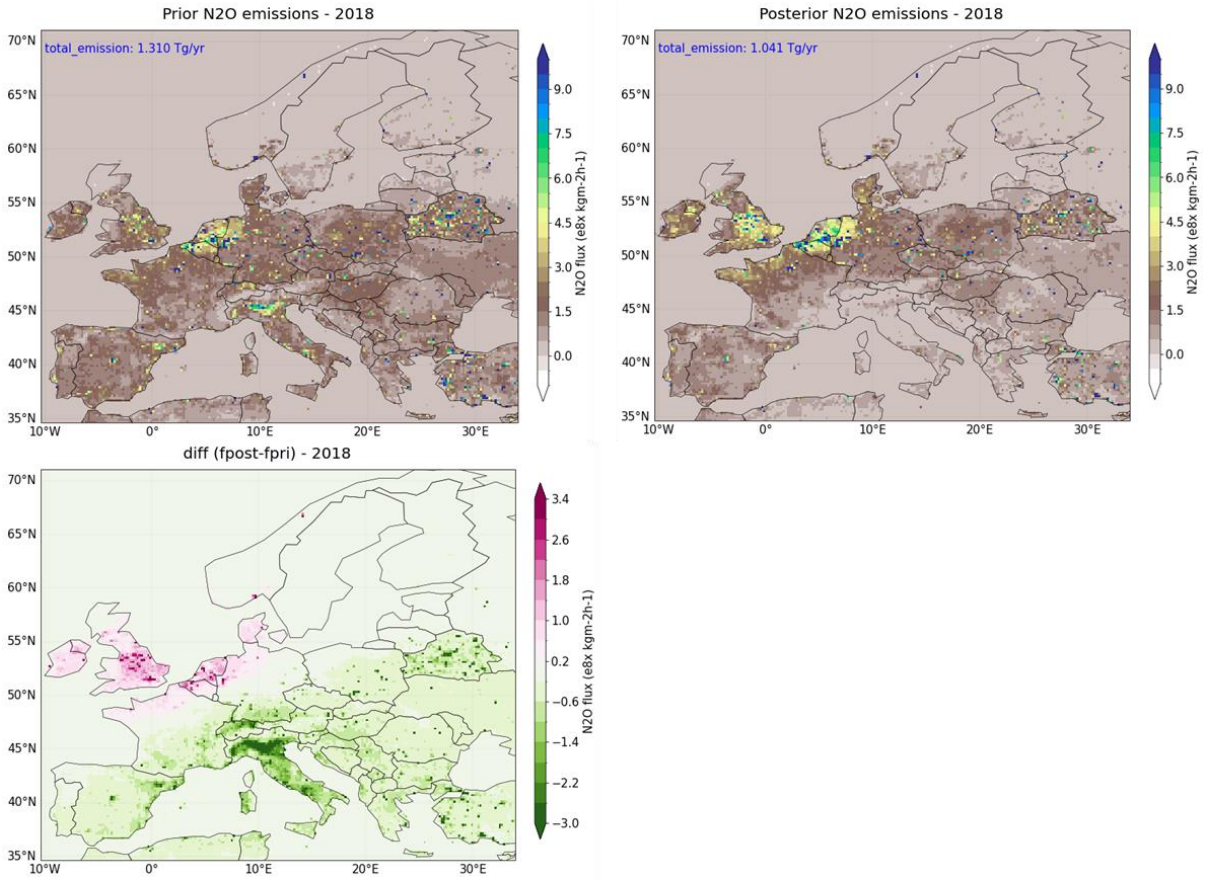

Figure 4.7: Annual mean spatial distribution of N_2O estimates from CIF-FLEXPART inversion at a higher resolution of 0.2°x 0.2° grid in the year 2018: prior (left upper panel), posterior (right upper panel) and posterior increments computed as (posterior – prior) (lower panel).

5. CO_2 inversions

This section describes the CIF-CHIMERE CO_2 inversion configuration at the relatively high resolution of 0.2° over Europe. This new high-resolution configuration presents several challenges. The main objective of our preliminary work with this high resolution was to assess the computational cost, as well as the impact of the high resolution of the transport model on the simulated CO_2 concentrations at local to continental scale. Such assessment has been made with simulations for the month of June 2019, when the posterior estimates from the surface measurements at the 0.5° spatial resolution identify a

This project has received funding from the European Union's Horizon Europe research and innovation programme under grant agreement No 101081395

CO_2 peak uptake (see deliverable D3.1) and is presented in this deliverable. The 1-month experiments conducted here are suitable for answering the key questions corresponding to this deliverable.

5.1 Experimental framework

The inversion system relies on the coupling between the variational mode of the CIF, Berchet et al., 2021), the regional chemistry transport model CHIMERE (Menut et al., 2013; Mailler et al., 2017) and the adjoint of this model (Fortems-Cheiney et al., 2021b).

5.1.1 Configuration of the regional CHIMERE CTM for the simulation of CO_2 concentrations over Europe

A European configuration of CHIMERE is used, covering latitudes 32.1-72.9°N and longitudes 14.9°W - 34.9°E with a 0.2°×0.2° horizontal resolution and 29 vertical layers up to 300 hPa. This domain is presented in Figure 5.1. This configuration corresponds to grid-cells of 250 (longitude) x 205 (latitude) x 29 (altitude) = 1 486 250, about 10 times higher than the one for the 0.5° configuration in D3.1 (with about 137 360 grid-cells).

At the time scales considered in this study, CO_2 is considered as a passive tracer. Consequently, when using the CHIMERE CTM and its adjoint code, here, only the atmospheric transport modeling components are used, and the chemistry modeling components are disactivated. Meteorological forcing for CHIMERE is generated using operational forecasts from the Integrated Forecasting System (IFS) of the European Centre for Medium Range Weather Forecasting (ECMWF).

5.1.2 CO_2 boundary conditions

Initial, lateral and top conditions for CO_2 concentrations at the boundaries of the model and at the simulations initial time are generated from the latest Copernicus Atmospheric Monitoring Service (CAMS) global CO_2 inversions (v22r1) assimilating surface data (Chevallier et al., 2005). This global inversion product is also used to complement the vertical columns of CO_2 above the top boundary of CHIMERE when comparing the model to XCO_2 observations.

5.2 Estimates of the CO_2 land ecosystem fluxes

A detailed assessment of the potential of having a 0.2° resolution for the overall inversion framework would benefit from using the "CRUERA" NBP coming from a European scale simulation run from 2005 to 2022 in the frame of the EYE-CLIMA project, with a dedicated forcing at the spatial resolution of 0.125°. This dataset is described in the Deliverable D2.3 of the EYECLIMA project. We have aggregated these fluxes at the 0.2°x0.2° horizontal resolution of the CHIMERE grid.

5.2.1. Other CO_2 surface fluxes

The other component of CO_2 fluxes from ocean and anthropogenic activities are fixed throughout the inversion. We have interpolated these fluxes at the 0.2°×0.2° horizontal resolution of the CHIMERE grid. The anthropogenic fossil fuel and biofuel CO_2 emissions (Gerbig and Koch, 2023) are based on the spatial distribution of the Emissions Database for Global Atmospheric Research EDGAR-v4.3 inventory (Janssens-Maenhout et al., 2019), on national and annual budgets from the BP (British Petroleum) statistics 2023, and on temporal profiles at hourly resolution derived from the TNO-MACC inventories, following the COFFEE approach (Steinbach et al., 2011). The data is provided from 2005 to 2022 at 0.1°×0.1°horizontal resolution and hourly temporal resolution. For the Deliverable D3.4 at month M28,

This project has received funding from the European Union's Horizon Europe research and innovation programme under grant agreement No 101081395

inversions will be performed with anthropogenic emissions from the EDGARv8 inventory, as recommended by WP2.

The estimate of sea/ocean fluxes within the CHIMERE domain is based on a hybrid product combining the coastal ocean flux estimates from the University of Bergen and a global ocean estimate from MPI-BGC-Jena (Rödenbeck et al., 2014; McGrath et al., 2023). The data is provided from 2005 to 2020 at a 0.125°×0.125° horizontal resolution and at daily temporal resolution.

Some CO_2 flux components are ignored in both these CHIMERE simulations and preliminary CIF-CHIMERE inversions: the biomass burning fluxes, and the fluxes associated to human/animal respiration, wood decomposition and lake/river outgassing. As stated above, these fluxes should be handled in a suitable way in the future series of reference inversions in D3.4.

5.3. Observations

The inversion assimilates measurements of CO_2 dry mole fraction from the European Obspack compilation of atmospheric carbon dioxide data from ICOS and non-ICOS European ground based continuous measurement stations for the period 1972-2022 called "obspackco2466GLOBALVIEWplusv8.02023-03-30" (ICOS RI et al., 2023). The location of the observations sites is presented in Figure 5.1.

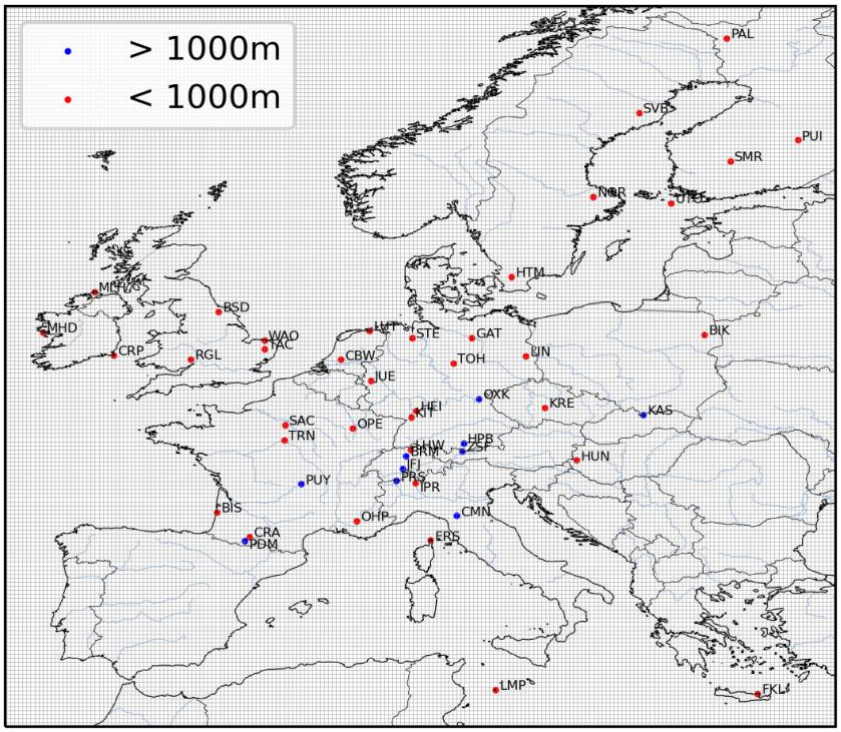

Figure 5.1: Domain and location of the observation sites. The colours indicate if the altitude (height above ground + sampling height) of the station is lower (in red) or higher (in blue) than 1000m.

ICOS-labelled stations have provided data since 2015. The database also includes measurements from non-labelled sites for the full period of inversion. However, before 2015, the data coverage is relatively sparse (Figure 3.2 of D3.1). Following usual observation selection strategies (Broquet et al., 2013, Monteil et al., 2020) the inversion assimilates 1-hour averages of the measured CO_2 mole fractions during the time windows 12:00-18:00 UTC for low altitude stations (below 1000 masl) and 0:00-7:00

This project has received funding from the European Union's Horizon Europe research and innovation programme under grant agreement No 101081395

UTC for high altitude stations (above 1000 masl). When several levels of measurements are available at a given station, the inversions assimilate the data from the highest level only.

5.4. Results

5.4.1. Comparison between simulations of the CO_2 mole fractions at the 0.2° and 0.5° spatial resolutions and observations

Comparisons between the bias and root mean square (RMS) differences (denoted RMS errors, i.e., RMSE) between the time series of measured and simulated concentrations both at the 0.5° and 0.2° spatial resolution are show in Figure 5.2, for each site, and for the entire ensemble of assimilated observations. The expectation is that the simulation at the 0.2° spatial resolution, particularly associated to a finer topography and to a finer representation of anthropogenic emissions over urban areas, should show a reduction of the misfits in terms of mean bias and RMSE compared to simulation at the 0.5° one.

Nevertheless, when taking the hourly observations of all the stations into account for the month of June 2019, the mean monthly bias between simulated versus measured CO_2 is slightly increased at the 0.2° resolution compared to the 0.5° resolution (mean bias of 1.98 ppm against 1.6 ppm, Table 5.1). The improvement of the fit to surface measurements with the simulation at relatively high resolution compared to the one at 0.5° resolution seems to depend on the station (Figure 5.2). The mean bias is indeed particularly surprisingly deteriorated at the urban station SAC (Saclay in France) and further work is needed to investigate these results. Without this station, the mean bias between simulated versus measured CO_2 are similar at the 0.5° and at the 0.2° resolution.

The mean monthly RMSE between simulated versus measured CO_2 is also slightly increased at the 0.2° resolution compared to the 0.5° resolution (mean bias of 5.71 ppm against 5.06 ppm, Table 5.1). However, except for the sites: BIK (in Poland), HEI (in Germany) and SAC, the RMSE are often very similar at the 0.2° and 0.5° resolution (Figure 5.2).

These first comparisons do not show a clear improvement, even a slight deterioration, of the fit to surface measurements with the simulation at relatively high resolution compared to the one at 0.5°. However, these statistics are only made for the month of June 2019. A full and detailed assessment of the potential of having a 0.2° resolution would have benefited from longer experiment, currently hampered by a high computational cost as seen in the following section.

Table 5.1. Statistics on the performance of the CHIMERE CTM using the CRUERA NEE fluxes compared to assimilated mole fraction measurements. Mean determinant coefficient (r^2), Root mean squared error (RMSE) and bias, considering all the hourly observations available in June 2019.

	r^2	**RMSE (ppm)**	**Bias (ppm)**
CRUERA Surface 0.5°	0.21	5.06	1.6
CRUERA Surface 0.2°	0.19	5.71	1.98

This project has received funding from the European Union's Horizon Europe research and innovation programme under grant agreement No 101081395

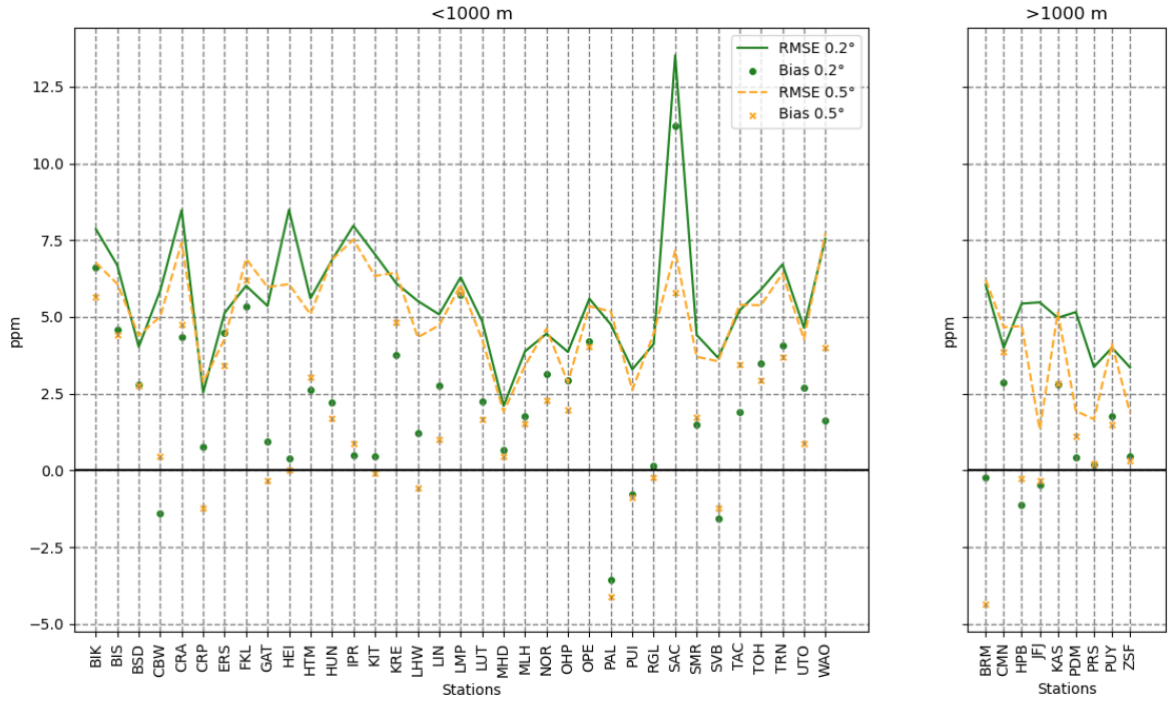

Figure 5.2: Forward simulation at 0.5° (orange) and 0.2° (green) mean bias (dots) and RMSE (solid lines) at observation site with altitude lower (left) and higher (right) than 1000m, in ppm, for the month of June 2019.

3.2.2. High computational cost preventing from performing long-term inversions

Different experiments have been first performed to assess the computational cost, as well as the impact of the high resolution of both the transport model and control of the fluxes on the simulated CO_2 concentrations at local to continental scale. Such experiments are presented in Table 5.2. Forward simulations have been performed both at the 0.5° and the 0.2° spatial resolution for the month of June 2019 and for the entire year 2019. Forward and adjoint cycles are also compared at the 0.5° and the 0.2° spatial resolution for the month of June 2019.

Table 5.2. Description of the experiments performed in this study and their associated computational cost.

Experiment	Period	Resolution	Number of processors	Total Computational cost
Forward Simulation	Year 2019	0.5°	10	1.3 days
Forward Simulation	Year 2019	0.2°	20	5.5 days
Cycle forward/adjoint	June 2019	0.5°	10	13 min
Cycle forward/adjoint	June 2019	0.2°	20	> 4 days

While a forward/adjoint cycle takes only 13 minutes with 10 processors at the 0.5° spatial resolution, a forward/adjoint cycle takes more than 4 days with 20 processors at the 0.2° spatial resolution (Table 5.2). This very high computational cost makes it difficult to perform inversions over longer periods at this stage. Technical developments on CHIMERE, in particular, porting the code to a GPU-compatible environment, are currently in progress to allow future series of reference long-term inversions in D3.4

This project has received funding from the European Union's Horizon Europe research and innovation programme under grant agreement No 101081395

due in M28. Preliminary results suggest a speeding up of the execution of the code by a factor of 6.5 in forward mode. However, further optimizations over the requested memory are still needed to accommodate carrying out adjoint simulations.

6. Deviations from the Description of Action

This deliverable is a step towards the main objective to perform high-resolution inversion of CO_2, CH_4 and N_2O over the Europe for at least the period 2018 to 2023. Presently, the inversions are performed from 2017 to 2022 for CH_4, and for 2018 for N_2O. The computation limitations and time taken to perform high-resolution inversion with the existing resources had a partial impact on completing more than one year of inversion.

For, N_2O inversions are performed using new versions of FLEXPART and CIF, which caused unforeseen delays in setting-up the model and test cases that were needed to ensure the quality of the results. However, the N_2O estimates for the following years will be included in the final inversion.

For CO_2, because of high computational cost, the assessment of the impact of the high resolution of the transport model on the simulated CO_2 concentrations and the associated computational cost has been only made with simulations for the month of June 2019. Technical developments on CHIMERE, particularly by porting the code to GPU-compatible environment, are currently in progress to allow future series of reference long-term inversions in D3.4 due in M28.

6.Conclusions

For CO_2, first comparisons over the month of June 2019 do not show a clear improvement, even a slight deterioration, of the fit to surface measurements with the simulation at relatively high resolution compared to the one at 0.5° and work is needed to understand this result. A full and detailed assessment of the potential of having a 0.2° resolution would have benefited from longer experiment, currently hampered by a high computational cost.

The CH_4 inversion over Europe was run for years 2017 to 2022. In this preliminary deliverable, we present the inversion results for 2019. The total emissions are optimised, and the posterior fluxes show large increases in Central Europe and large reductions in Italy, Romania and UK and modest reductions in northern Europe during summer, compared to the prior estimates. The reductions are most probably due to too large prior estimates for geological emissions in southern Europe. For the final deliverable we will optimise different emission components including geological, wetland, and biogenic and non-biogenic anthropogenic emissions. Observations from ground-based measurement stations, including all ICOS sites, was used in flux optimisation. We will next assimilate TROPOMI satellite data in CIF-FLEXPART to improve the spatial constraints for the high-resolution inversion.

The N_2O inversion is performed over the European domain for 2018. The results show good agreement between observations and posterior mixing ratios. The optimised emissions are overall lower than the prior estimate (~21%). Most of the reductions in emissions are concentrated near Italy, in Central and Eastern Europe, while there are some regions, particularly in Northwestern Europe (such as the UK and parts of France) and regions around Netherlands where the emissions increased.

The high-resolution inversions presented in this task represent significant technical challenges compared to the 0.5°×0.5° inversions described in D3.1. The improvement in performance compared to the 0.5° inversions will be more thoroughly examined in the next inversion deliverables in 2025.

This project has received funding from the European Union's Horizon Europe research and innovation programme under grant agreement No 101081395

7. References

Berchet, A., Sollum, E., Thompson, R. L., Pison, I., Thanwerdas, J., Broquet, G., Chevallier, F., Aalto, T., Berchet, A., Bergamaschi, P., Brunner, D., Engelen, R., Fortems-Cheiney, A., Gerbig, C., Groot Zwaaftink, C. D., Haussaire, J.-M., Henne, S., Houweling, S., Karstens, U., Kutsch, W. L., Luijkx, I. T., Monteil, G., Palmer, P. I., van Peet, J. C. A., Peters, W., Peylin, P., Potier, E., Rödenbeck, C., Saunois, M., Scholze, M., Tsuruta, A., and Zhao, Y.: The Community Inversion Framework v1.0: a unified system for atmospheric inversion studies, Geoscientific Model Development, 14, 5331–5354, https://doi.org/10.5194/gmd-14-5331-2021, 2021.

Bergamaschi, P., Karstens, U., Manning, A. J., Saunois, M., Tsuruta, A., Berchet, A., Vermeulen, A. T., Arnold, T., Janssens-Maenhout, G., Hammer, S., Levin, I., Schmidt, M., Ramonet, M., Lopez, M., Lavric, J., Aalto, T., Chen, H., Feist, D. G., Gerbig, C., Haszpra, L., Hermansen, O., Manca, G., Moncrieff, J., Meinhardt, F., Necki, J., Galkowski, M., O'Doherty, S., Paramonova, N., Scheeren, H. A., Steinbacher, M., and Dlugokencky, E.: Inverse modelling of European CH4 emissions during 2006–2012 using different inverse models and reassessed atmospheric observations, Atmospheric Chemistry and Physics, 18(2), 901-920, https://doi.org/10.5194/acp-18-901-2018, 2018.

Etiope, G., Ciotoli, G., Schwietzke, S., & Schoell, M.: Gridded maps of geological methane emissions and their isotopic signature, Earth System Science Data, 11(1), 1-22, https://doi.org/10.5194/essd-11-1-2019, 2019.

Errico, R. M.: What is an adjoint model?, Bulletin of the American Meteorological Society, 78(11), 2577-2591, 1997.

Hittmeir, S., Philipp, A., Seibert, P., & Makovec, F.: Preprocessing of meteorological data for Lagrangian modeling, Geoscientific Model Development, 11(7), 2739-2749, https://doi.org/10.5194/gmd-11-2739-2018, 2018.

Lanczos, C.: An iteration method for the solution of the eigenvalue problem of linear differential and integral operators, Journal of Research of the National Bureau of Standards, 45(4), 255-282, https://doi.org/10.6028/jres.045.026, 1950.

Meirink, J. F., Bergamaschi, P., and Krol, M. C.: Four-dimensional variational data assimilation for inverse modelling of atmospheric methane emissions: method and comparison with synthesis inversion, Atmospheric Chemistry and Physics, 8(21), 6341–6353, https://doi.org/10.5194/acp-8-6341-2008, 2008.

Petrescu, A. M. R., McGrath, M. J., Andrew, R. M., Peylin, P., Peters, G. P., Ciais, P., Broquet, G., Tubiello, F. N., Gerbig, C., Pongratz, J., Janssens-Maenhout, G., Grassi, G., Nabuurs, G.-J., and Dolman, A. J.: The consolidated European synthesis of CH4 and N2O emissions for the European Union and United Kingdom: 1990–2017, Earth System Science Data, 13(5), 2307–2362, https://doi.org/10.5194/essd-13-2307-2021, 2021.

Pisso, I., Sollum, E., Grythe, H., Kristiansen, N. I., Cassiani, M., Eckhardt, S., Arnold, D., Morton, D., Thompson, R. L., Zwaaftink, C. D. G., Evangeliou, N., Sodemann, H., Haimberger, L., Henne, S., Brunner, D., Burkhart, J. F., Fouilloux, A., Brioude, J., Philipp, A., Seibert, P., & Stohl, A.: The Lagrangian particle dispersion model FLEXPART version 10.4, Geoscientific Model Development, 12(12), 4955-4997, https://doi.org/10.5194/gmd-12-4955-2019, 2019.

Randerson, J. T., van der Werf, G. R., Giglio, L., Collatz, G. J., & Kasibhatla, P. S.: Global Fire Emissions Database, Version 4.1 (GFEDv4), ORNL DAAC, https://doi.org/10.3334/ORNLDAAC/1293, 2017.

This project has received funding from the European Union's Horizon Europe research and innovation programme under grant agreement No 101081395

Saunois, M., Martinez, A., Poulter, B., Zhang, Z., Raymond, P., Regnier, P., Canadell, J.G., Jackson, R.B., Patra, P.K., Bousquet, P., Ciais, P., Dlugokencky, E.J., Lan, X., Allen, G.H., Bastviken, D., Beerling, D.J., Belikov, D.A., Blake, D.R., Castaldi, S., Crippa, M., Deemer, B.R., Dennison, F., Etiope, G., Gedney, N., Höglund-Isaksson, L., Holgerson, M.A., Hopcroft, P.O., Hugelius, G., Ito, A., Jain, A.K., Janardanan, R., Johnson, M.S., Kleinen, T., Krummel, P., Lauerwald, R., Li, T., Liu, X., McDonald, K.C., Melton, J.R., Mühle, J., Müller, J., Murguia-Flores, F., Niwa, Y., Noce, S., Pan, S., Parker, R.J., Peng, C., Ramonet, M., Riley, W.J., Rocher-Ros, G., Rosentreter, J.A., Sasakawa, M., Segers, A., Smith, S.J., Stanley, E.H., Thanwerdas, J., Tian, H., Tsuruta, A., Tubiello, F.N., Weber, T.S., van der Werf, G., Worthy, D.E., Xi, Y., Yoshida, Y., Zhang, W., Zheng, B., Zhu, Qing, Zhu, Qiuan, Zhuang, Q., Global Methane Budget 2000-2020. Earth System Science Data Discussions 1–147. https://doi.org/10.5194/essd-2024-115, 2024.

Stohl, A., Wotawa, G., Seibert, P., & Kromp-Kolb, H.: Interpolation errors in wind fields as a function of spatial and temporal resolution and their impact on different types of kinematic trajectories, Journal of Applied Meteorology, 34(10), 2149-2165, https://doi.org/10.1175/1520-0450(1995)034<2149>2.0.CO;2, 1995.

Thompson, R. L., & Stohl, A.: COCCON: an international network to detect changes in carbon monoxide, Atmospheric Chemistry and Physics, 14(5), 2319-2342, https://doi.org/10.5194/acp-14-2319-2014, 2014.

Tipka, A., Hittmeir, S., Philipp, A., & Seibert, P.: Flex_extract v7.1.2 - a software package to retrieve and prepare ECMWF data for use in FLEXPART, Geoscientific Model Development, 13(11), 5277-5310, https://doi.org/10.5194/gmd-13-5277-2020, 2020.

Weber, T.: Estimates of global ocean methane emissions based on a spatially explicit global ocean methane model, Biogeosciences, 16(17), 3227-3244, https://doi.org/10.5194/bg-16-3227-2019, 2019.

This project has received funding from the European Union's Horizon Europe research and innovation programme under grant agreement No 101081395

https://eyeclima.eu

BRUSSELS, 19 09 2024

Funded by the European Union. Views and opinions expressed are however those of the author(s) only and do not necessarily reflect those of the European Union. Neither the European Union nor the granting authority can be held responsible for them.

This project has received funding from the European Union's Horizon Europe research and innovation programme under grant agreement No 101081395